Catena 147 (2016) 177–186

Contents lists available at ScienceDirect

Catena

journal homepage: www.elsevier.com/locate/catena

Spatial distribution and temporal trends of rainfall erosivity in mainland China for 1951–2010

Wei Qin [a,b,*], Qiankun Guo [a,b], Changqing Zuo [a,b], Zhijie Shan [a,b], Liang Ma [c], Ge Sun [d]

[a] State Key Laboratory of Simulation and Regulation of Water Cycle in River Basins, China Institute of Water Resources and Hydropower Research, 100048 Beijing, PR China
[b] Research Center of Soil and Water Conservation of the Ministry of Water Resources, 100048 Beijing, PR China
[c] Water Resources Research Institute of Shandong Province, 250013 Ji'nan, Shandong, PR China
[d] Eastern Forest Environmental Threat Assessment Center, Southern Research Station, USDA Forest Service, 27606 Raleigh, NC, USA

ARTICLE INFO

Article history:
Received 24 February 2016
Received in revised form 23 May 2016
Accepted 5 July 2016
Available online xxxx

Keywords:
Rainfall erosivity
Spatial distribution and temporal trends
Kendall slope
Mainland China
Soil erosion regions

ABSTRACT

Rainfall erosivity is an important factor for estimating soil erosion rates. Understanding the spatial distribution and temporal trends of rainfall erosivity is especially critical for soil erosion risk assessment and soil conservation planning in mainland China. However, reports on the spatial distribution and temporal trends of rainfall erosivity for China, especially of its eight soil erosion regions, are still lacking, which reduces the accuracy of predicting soil losses, assessing soil erosion risks and evaluating the effects of soil conservation measures. Additionally, the lack of the most suitable spatial interpolation method in mainland China, to some degree, has reduced the applicability and reliability of the interpolation results. In this study, long-term (1951–2010) daily rainfall data from 756 national weather stations were assembled to characterize the spatial and temporal patterns of annual rainfall erosivity across mainland China. Sixteen spatial interpolation methods were compared to select the most suitable one for accurately mapping the spatial distribution of rainfall erosivity, and the Mann-Kendall test was employed to detect the temporal trends. The results indicated that 1) the universal co-kriging method with the aid of elevation was superior to the other spatial interpolation methods; 2) long-term average rainfall erosivity increased from the northwest to the southeast, ranging from 31 to 30,051 MJ mm $ha^{-1} h^{-1} a^{-1}$; 3) overall, rainfall erosivity across China and water erosion regions experienced an insignificant increasing trend over the study period. Significant decreasing trends were observed in the northwest Loess Plateau region (0.01 level), the northeast black soil region and the north earth and gravel mountain region (0.05 level). Significant increasing trends (0.05 level) were found in the southern red soil hilly region and the southwest Karst region; and 4) two lines were identified according to the temporal trends of rainfall erosivity from the east to the west. In total, this study offers useful information both for soil erosion prediction and land management practices of mainland China.

© 2016 Elsevier B.V. All rights reserved.

1. Introduction

Soil erosion is universally recognized as a serious threat to man's well-being (Hudson, 1995). The most commonly used methods for predicting soil erosion is the Universal Soil Loss Equation (USLE) (Wischmeier and Smith, 1965, 1978) and the Revised USLE (RUSLE) (Renard et al., 1997). In the USLE and RUSLE, the rainfall erosivity factor (R) represents the climatic influence on water-related soil erosion (Lu and Yu, 2002). The spatial and temporal distributions of rainfall erosivity can be used as indicators of regional variations in erosion potential (Morgan, 2005).

The spatial distributions of rainfall erosivity have been widely reported in many countries, including China, both on the national and regional scales (Table 1). However, the spatial distribution of rainfall erosivity in terms of soil erosion regions in mainland China has not been reported until now, and to some degree, this reduces the accuracy of predicting soil losses and assessing soil erosion risks. The concept of a "soil erosion region" was widely used in China, and such regions were determined according to the synthesis analysis of factors affecting soil erosion, such as the soil type, topography, climate, and so on. A soil erosion region is the primary administration unit allocating soil conservation resources, soil erosion inventory, and soil conservation planning; thus, knowing the spatial distribution of the rainfall erosivity of soil erosion regions is critical.

Temporal changes of rainfall erosivity have also been noted by researchers, especially under the circumstances of global climate change (Nearing, 2001; Sun et al., 2002; Segura et al., 2014). The most consequential effects of climate change on water erosion are the changes of erosive power or erosivity (Nearing, 2001), which can influence the extent, frequency and magnitude of soil erosion (Williams et al., 1996), and have significant impacts on soil erosion rates (Nearing et al., 2004). Potential changes of rainfall erosivity under future climatic scenarios on the national scale, such as in the United States (Nearing,

* Corresponding author.
E-mail address: qinwei@iwhr.com (W. Qin).

http://dx.doi.org/10.1016/j.catena.2016.07.006
0341-8162/© 2016 Elsevier B.V. All rights reserved.

Table 1
Summaries of relevant studies on spatial and temporal distribution of rainfall erosivity. In the "Key results" section, three components are identified by the codes: 1) explore the suitable methods for spatial interpolation in study region; 2) present the spatial distribution of rainfall erosivity in study region (range of rainfall erosivity, MJ mm ha^{-1} h^{-1} a^{-1}); 3) characterize the temporal trends of rainfall erosivity in study region. Note that many studies do not assess all three components and N/A directly follows the codes in such cases.

Study	Location	Data/methods	Key results
Angulo-Martínez and Beguería (2012)	Elbro Valley, Spain, 85,000 km^2	Data: 156 sites, 1955–2006 daily rainfall series 110 sites, 1997–2006 15 min resolution R calculation: RUSLE method and daily rainfall model	1. Local interpolation methods (Inverse distance weighting and spline) yield the best results 2. Spatial distribution was presented: 300 to 2700
Angulo-Martínez et al. (2009)		Interpolation: generalized least square; inverse distance weighting and spline; ordinary, universal and co-kriging	3. General decrease in annual and seasonal rainfall erosivity
Bonilla and Vidal (2011)	Central Chile	Data:16 stations continuous record; 241 annual rainfall R calculation: annual model Interpolation: kriging	1. N/A 2. Spatial distribution was presemted: 90 to 7375 3. N/A
Hoyos et al. (2005)	Dosquebrade Basin, Colombia, 58 km^2	Data: 6 stations, 1987–1997, pluviograph data R calculation: RUSLE method, missing R was estimated by daily rainfall model (threshold daily rainfall: 12.7 mm) Interpolation: inverse distance weighted; local polynomial	1. Local polynomical is better 2. Spatial distribution was presented: 10,409 to 15,975 3. N/A
Lu and Yu (2002)	Australia	Data: 132 sites, 1980–1999 daily rainfall, 0.05° resolution R calculation: daily model Interpolation: ordinary kriging	1. N/A 2. Spatial distribution was presented: 234 to 40,000 3. N/A
Meusburger et al. (2012)	Switzerland	Data: 71 sites, 1989–2010 10 min resolution R calculation: RUSLE method, threshold 8.47 mm/20 min Interpolation: regression kriging	1. Regression Kriging seemed to be the best choice 2. Spatial distribution was presented: 124 to 5611 3. Significant increasing trend for May to October and significant decreasing trend in February
Santasa et al. (2010)	Hitotsuse basin, Kyushu, Japan	Data: 8 stations, 9–17 years period with 10 min interval R calculation: RUSLE method Interpolation: kriging, spline, inverse distance weighting	1. Inverse Distance Weighting is more appropriate 2. Spatial distribution was presented: 7775 to 10,235 3. N/A
de Silva (2004)	Brazil	Data: 1600 weather stations, 20 years' pluviometric records R calculation: eight models for eight regions. Interpolation: not mentioned	1. N/A 2. Spatial distribution was presented: 3116 to 20,035 3. N/A
Huang et al. (2013)	Yangtze river basin, China, 1808,500 km^2	Data: 146 stations, 1960–2005 daily rainfall data R calculation: same as in this study Interpolation: inverse distance weighted	1. N/A 2. Spatial distribution was presented: 131.2 to 16,842 3. Upward trends for most stations
Liu et al. (2013a)	China	Data: 590 meteorological stations, 1960–2009 daily data R calculation: same as in this study Interpolation: ordinary kriging	1. N/A 2. Spatial distribution was presented: <50 to >14,000 3. Slight increase in most parts of China
Ma et al. (2014)	Kejie watershed, 1755 km^2 Yunnan, China	Data: 5 stations, 1965–2010 daily rainfall data R calculation: three models used in this study Interpolation: co-kriging	1. N/A 2. Spatial distribution was presented: 2505 to 5538 3. No significant increasing or decreasing trend observed
Men et al. (2008)	Hebei, China, 188,900 km^2	Data: 373 stations, 1961–2000, 62 stations daily rainfall data R calculation: daily model same as in this study Interpolation: ordinary, simple, logarithm normal, universal, disjunctive kriging and inverse distance weighted	1. Disjunctive Kriging was the best method. 2. Spatial distribution was presented: 929.7 to 16,670 3. N/A
Xin et al. (2011)	Loess Plateau, China, 64×10^4 km^2	Data: 87 stations, 1956–2008 daily rainfall data R calculation: same as in this study Interpolation: inverse distance weighted	1. N/A 2. Spatial distribution was presented: 220 to 2200 3. Decrease over the past five decades
Yang and Lu (2015)	Dryland region, China 5.6 million km^2	Data: 298 stations, 1961–2002, daily rainfall data R calculation: Same as in this study Interpolation: a quadratic polynomial equation	1. N/A 2. Spatial distribution was presented: 2 to 4098 3. Upward trend for arid zone, no evident trend for semi-arid zone, downward trend for sub-humid zone
Zhu and Yu (2015)	China	Data: 22 stations, 1956–1984, pluviograph data R calculation: monthly and daily model Interpolation: a quadratic polynomial equation	1. N/A 2. Spatial distribution was presented: <10 to >10,000 3. N/A

2001) and China (Sun et al., 2002), and on the regional scale, such as in the Yellow River Basin of China (Zhang et al., 2005) and the north Rhine Westphalia of Germany (Sauerborn et al., 1999), have been studied. However, detailed studies on temporal changes of rainfall erosivity in soil erosion regions in China are also lacking. It can be seen that both the spatial distribution and temporal trends of rainfall erosivity in mainland China have not previously been reported, which indicates that there is a need to fill the knowledge gap to provide better guidance for soil conservation management of different soil erosion regions in China.

It is also very practical to assess the spatial distribution and temporal trends of rainfall erosivity in mainland China. As is known, the Chinese government has implemented a series of policies towards ecological restoration across a variety of spatial-temporal scales, including adoption of numerous soil conservation measures to increase vegetation cover, optimize land use patterns and reduce soil loss rates. Accurately quantifying the effectiveness of these measures is of great significance for allocating limited resources to achieve better soil conservation results, which is necessary to eliminate the effects of spatial and temporal changes of rainfall erosivity on soil loss, especially under the conditions of substantial increases or decreases of rainfall for different regions in mainland China that have been reported (Gemmer et al., 2004; Zhang et al., 2009; Xiao et al., 2013) because rainfall erosivity is calculated based on the rainfall data. The spatial distribution and temporal trends of rainfall erosivity in mainland China are critical for accurately assessing the effects of soil conservation measures.

Another problem that remains unresolved is although the spatial distributions of rainfall erosivity have been reported in many studies, only a small proportion of these studies compared the effectiveness of different interpolation methods, and most comparisons were made

between a limited numbers of interpolation methods (Table 1); hence, it is necessary to determine the most suitable spatial interpolation method of rainfall erosivity in mainland China. For spatial interpolation, it is critical to capitalize on any source of information to predict rainfall erosivity at unmonitored locations because rainfall erosivity is only available at a limited number of locations (Goovaerts, 1999). Thus, it is necessary to compare the applicability and reliability of the commonly used interpolation methods to find the most suitable one to obtain the best estimation of rainfall erosivity.

In this study, the spatial and temporal distributions of rainfall erosivity in mainland China and different soil erosion regions were studied. The specific objectives are 1) to explore the suitable methods for spatial interpolation; 2) to present the spatial distribution of rainfall erosivity in mainland China and soil erosion regions; and 3) to characterize the temporal trends of rainfall erosivity in mainland China and its soil erosion regions. The results in this study offer information on the soil erosion potential in mainland China and its soil erosion regions and provide a reference for soil erosion prediction and evaluation of the effectiveness of current soil conservation measures.

2. Materials and methods

The observed daily precipitation data used in this study was obtained from the Climatic Data Center, National Meteorological Information Center of the China Meteorological Administration (CMA) (http://data.cma.gov.cn). The data were collected from 756 national meteorological stations in China (excluding Hong Kong, Macau and Taiwan), covering the period from 1950 to 2010. This is one of the largest rainfall databases used for calculating rainfall erosivity in mainland China.

2.1. Rainfall erosivity calculation

Because continuous rainfall data series with a high time resolution for calculating USLE rainfall erosivity factor are rarely available, daily rainfall data have been widely used worldwide to estimate rainfall erosivity (Table 1). In China, attempts to estimate rainfall erosivity from annual, monthly and daily rainfall were made by Zhang and Fu (2003), and the results indicated that the performance of daily rainfall data was obviously better, with an average relative error for estimating average annual rainfall erosivity of only 4.2%. A daily rainfall model was proposed by Zhang et al. (2002), which was subsequently widely used in China (Table 1). The equation is

$$R_i = \rho \sum_{j-1}^{k} (D_j)^{\sigma} \tag{1}$$

where R_i is the rainfall erosivity of the ith half-month of the year, MJ mm ha^{-1} h^{-1}; k is the number of days in the ith half-month; D_j is the effective rainfall for day j in one half-month; and D_j is the actual rainfall when the actual rainfall is higher than 12 mm; otherwise, D_j is considered to be 0. The term ρ and σ are parameters determined by the following formulas:

$$\sigma = 0.8363 + 18.144 {P_{d12}}^{-1} + 24.455 {P_{y12}}^{-1} \tag{2}$$

$$\rho = 21.586 \sigma^{-7.1891} \tag{3}$$

where P_{d12} and $P_{y12}$are the average daily and annual rainfall for days with rainfall >12 mm, respectively.

Rainfall records were not available at some stations for several years. The missing daily rainfall data were interpolated using the inverse distance weighted method according to the rainfall data of neighboring stations.

2.2. Comparison and selection of spatial interpolation methods

Sixteen spatial interpolation methods were used in this study to present the spatial distribution of rainfall erosivity (Table 2). These methods can be classified into four types: polynomial interpolation (PI), including global polynomial and local polynomial interpolation; inverse distance weighting (IDW); radial basis function (RBF), including thin plate spline, spline with tension, completely regularized spline, multiquadric spline, and inverse multiquadric spline; and kriging interpolation (KI), including ordinary kriging, simple kriging, universal kriging, disjunctive kriging and co-kriging. There are also four methods of co-kriging: ordinary, simple, universal and disjunctive. For kriging interpolation, the elevation of each weather station was used to aid the geostatistical mapping of rainfall erosivity because the interpolation results using co-kriging with a secondary datum, such as elevation, were better than those of other simple kriging methods (Goovaerts, 1999).

Spatial interpolation of rainfall erosivity based on the 602 randomly selected stations, accounting for 80% of the total 756 stations, was performed using all of the interpolation methods listed above for the years 1951, 1956, 1961, 1966, 1971, 1976, 1981, 1986, 1991, 1996, 2001 and 2006 to choose the most suitable interpolation method. Then, the interpolation results of the remaining 154 stations of each method were compared with the erosivity calculated by Eq. (1). Cross validation was used to compare the performances of various interpolation methods to select the best one. Cross validation is a commonly applied method in geostatistics, which is usually determined by the following indexes: mean relative error (*MRE*), determination coefficient (r^2) and the Nash-Sutcliffe efficiency coefficient (E_{ns}) (Nash and Sutcliffe, 1970). These indexes are calculated using the following equations:

$$MRE = \frac{1}{n} \sum_{i-1}^{n} \left| \frac{O_i - P_i}{O_i} \right| \tag{4}$$

$$r^2 = \frac{\left(\sum_{i=1}^{n} \left(O_i - \overline{O} \right)(P_i - \overline{P}) \right)^2}{\sum_{i=1}^{n} \left(O_i - \overline{O} \right)(P_i - \overline{P})^2} \tag{5}$$

$$E_{ns} = 1 - \frac{\sum_{i=1}^{n} (P_i - \overline{P})^2}{\sum_{i=1}^{n} \left(O_i - \overline{O} \right)^2} \tag{6}$$

Table 2
Comparison and selection of the interpolation methods.

Interpolation methods		*MRE*	r^2	E_{ns}
Polynomial interpolation	Global PI	6.04 ± 2.00	0.53 ± 0.04	0.53 ± 0.04
	Local PI	0.66 ± 0.24	0.80 ± 0.04	0.80 ± 0.04
Inverse distance weighted	IDW	0.69 ± 0.23	0.78 ± 0.04	0.79 ± 0.04
Radial basis function	Thin plate spline	0.67 ± 0.19	0.74 ± 0.05	0.73 ± 0.06
	Spline with tension	0.69 ± 0.23	0.81 ± 0.04	0.80 ± 0.04
	Completely regularized spline	0.68 ± 0.23	0.78 ± 0.08	0.75 ± 0.15
	Multiquadric spline	0.62 ± 0.20	0.79 ± 0.05	0.78 ± 0.05
	Inversed multiquadric spline	0.75 ± 0.26	0.77 ± 0.08	0.74 ± 0.16
Kriging	Ordinary kriging	0.63 ± 0.20	0.78 ± 0.05	0.77 ± 0.04
	Simple kriging	0.82 ± 0.24	0.79 ± 0.04	0.67 ± 0.08
	Universal kriging	0.62 ± 0.20	0.77 ± 0.04	0.78 ± 0.03
	Disjunctive kriging	0.82 ± 0.24	0.79 ± 0.04	0.67 ± 0.08
Co-kriging	Ordinary co-kriging	0.60 ± 0.19	0.81 ± 0.04	0.79 ± 0.06
	Simple co-kriging	0.66 ± 0.24	0.79 ± 0.06	0.75 ± 0.05
	Universal co-kriging	**0.60 ± 0.19**	**0.81 ± 0.04**	**0.81 ± 0.06**
	Disjunctive co-kriging	0.66 ± 0.23	0.81 ± 0.06	0.77 ± 0.04

where P_i and O_i are the simulated and measured rainfall erosivity for station i, respectively, $\overline{P}$ and $\overline{O}$ are the average simulated and measured values, respectively, and n is the number of data. Lower *MRE* yields better interpolation method performances. E_{ns} and r^2 should be higher than 0.5 and 0.6, respectively (Zheng et al., 2010).

2.3. Spatial distribution of rainfall erosivity

The best simulation method, determined by comparing *MRE*, E_{ns} and r^2, was used to interpolate the spatial distribution of rainfall erosivity. Usually spatial distribution of the long-term average annual rainfall erosivity was obtained by interpolating the long-term average annual rainfall erosivity of each station. Despite its simplicity, this method probably loses the chronological information of rainfall erosivity, thereby reducing the reliability of the interpolation results. Thus, another approach was chosen in this study: first, the spatial distribution of rainfall erosivity for each year from 1951 to 2010 was interpolated using the best interpolation method determined above. Then, the spatial distribution for the 60-year period (1951–2010) and each decade, i.e., 1951–1960, 1961–1970, 1971–1980, 1981–1990, 1991–2000 and 2001–2010, were obtained by averaging the interpolation results of the corresponding years. For example, the spatial distribution of rainfall erosivity for 1951–1960 was acquired by averaging 10 years (1951–1960) of interpolation results.

Considering the great internal geographical differences, China has adopted soil erosion regions for soil erosion research, soil erosion inventories and soil conservation planning. The soil erosion regions were delineated according to the synthesis analysis of factors affecting soil erosion, such as soil type, topography, and climate. These regions include the northeast black soil region (NE), the northern sandy region (NS), the north earth and gravel mountain region (N), the northwest Loess Plateau region (NW), the southern red soil hilly region (S), the southwest purple soil region (SW), the southwest Karst region (SK) and the Qinghai-Tibet Plateau region (QT) (Fig. 1). Water erosion is the dominant erosion form in all regions, except for NS and QT, whereas wind erosion mainly occurs in NS and freeze-thaw erosion occurs in QT. The spatial distribution of rainfall erosivity in each region was also calculated to present the regional differences.

2.4. Temporal changes of rainfall erosivity

The 3-year moving average rainfall erosivity was used to analyze the temporal changes across China and soil erosion regions because there was a 3–4 year periodicity of the change of annual precipitation (Wang et al., 2012) in most regions of China that could smooth the fluctuations and reduce the potential errors. The Mann-Kendall test (Mann, 1945) was used to identify temporal trends of rainfall erosivity, which is thought to be more suitable to assess the significance of trends in hydrometeorological time series, such as water quality, stream flow, temperature and precipitation (Yue et al., 2002), and is highly recommended for general use by the World Meteorological Organization (Mitchell et al., 1966). The tests were performed for both the 60-year period and different decades across China and for different erosion regions. There were two useful indexes in the Mann-Kendall test: z and β. A positive z value indicates an increasing trend, whereas a negative value indicates a decreasing trend. The trend is statistically significant at the 0.1, 0.05 and 0.01 significance level when $|z|>1.645$, 1.96 and 2.576, respectively. β is the Kendall slope, which indicates the magnitude of monotonic change (Xu et al., 2003). The detailed procedure of the MK trend test is presented in Huang et al. (2013). The turning points of temporal trends were detected using the sequential Mann-Kendall test. The points were defined by the intersections of the so-called progressive and retrograde series of the sequential Mann-Kendall test (Sneyers, 1990).

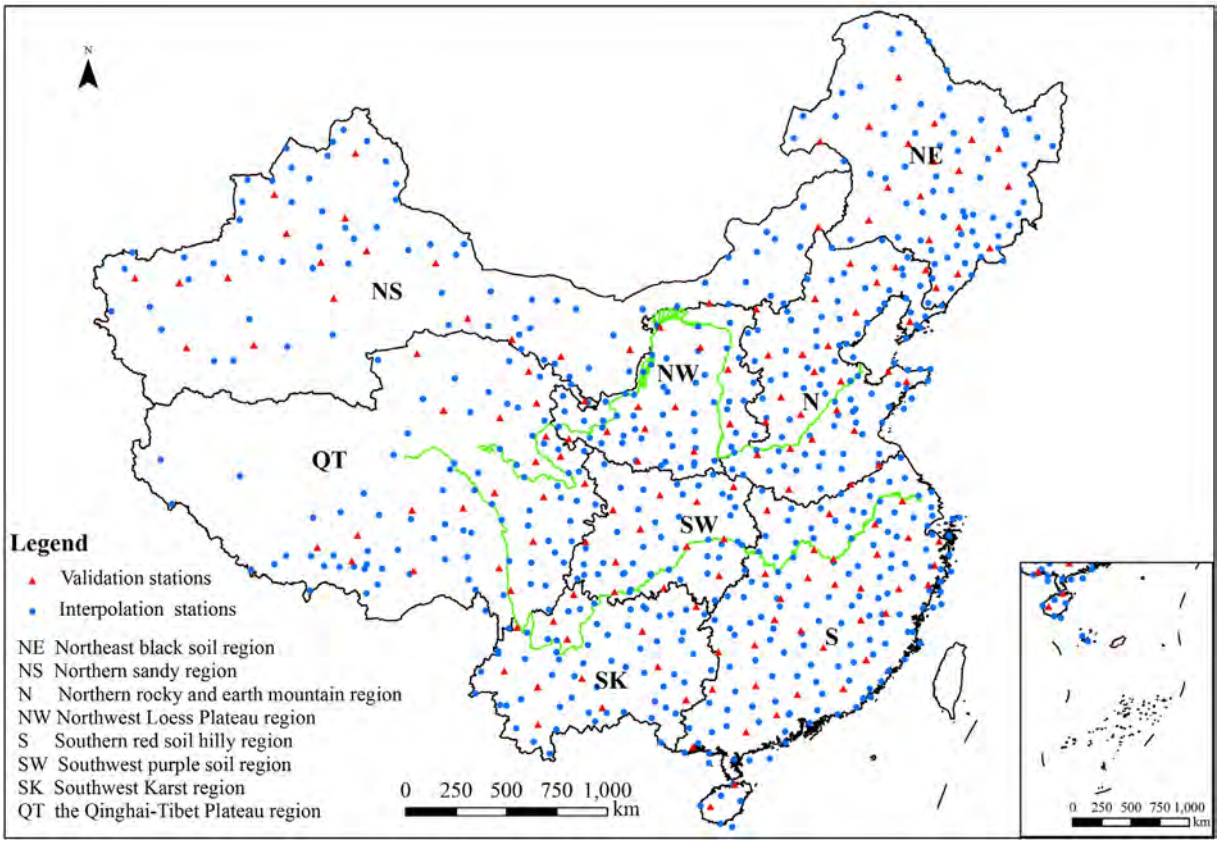

Fig. 1. Geographic distribution of soil erosion regions and weather stations in mainland China.

2.5. Spatial-temporal changes of rainfall erosivity

The internal variability of temporal changes of rainfall erosivity in mainland China was determined by the following method: first, β values for each weather station during 1951–2010 were calculated; then, the spatial distribution of β values was interpolated to present the spatial-temporal trends of rainfall erosivity, which can provide more detailed information on the geographic distribution of changing trends throughout the country.

3. Results

3.1. Selection of spatial interpolation methods

The values of *MRE*, E_{ns} and $r^2$of different interpolation methods are listed in Table 2. Obviously, the performances of the co-kriging methods were better than those of other methods, with the lowest *MRE* (0.60–0.66) and highest E_{ns}(0.79–0.81) and r^2(0.75–0.81) of all of the methods. The universal co-kriging method is the most suitable method of all of the co-kriging methods because its *MRE* (0.60) was the lowest and its E_{ns} and r^2 (both 0.81) were the highest.

3.2. Spatial distribution of rainfall erosivity

The spatial distribution of the 60-year annual rainfall erosivity is presented in Fig. 2. It can be concluded that annual rainfall erosivity increased from northwest to southeast, ranging from 30.7 to 30,051.1 MJ mm ha^{-1} h^{-1} a^{-1}. Rainfall erosivity was lowest (158.5 MJ mm ha^{-1} h^{-1} a^{-1}) in NW and highest (9480.9 MJ mm ha^{-1} h^{-1} a^{-1}) in S (Table 3). Rainfall erosivity in S was approximately twice that of SW and SK, both located in south China; approximately three times higher than that of N, mainly in north China; approximately six times higher than that of NE; and approximately eight times higher than that of NW. The rainfall erosivities of TP and NS were only 5% and 2% that of S, respectively, indicating substantial differences among soil erosion regions (Table 3). The spatial distribution of rainfall erosivity in China is similar with the geographic distribution of rainfall (Gemmer et al., 2004; Zhang et al., 2009).

3.3. Temporal changes of rainfall erosivity

The average annual rainfall erosivity from 1950 to 2010 was 2434 MJ mm ha^{-1} h^{-1} a^{-1}, with the lowest value of 2124 MJ mm ha^{-1} h^{-1} a^{-1} in 1978 and highest value of 2950 MJ mm ha^{-1} h^{-1} in 1998. A 60-year insignificant increasing trend was reported (Table 4); however, the trends were different for different decades: insignificant decreasing trends were observed for three decades (1961–1990), whereas increasing trends were observed in the first decade (1951–1960) and the last two decades (1991–2010). A significant increasing trend (0.01 level) for 1991–2010 probably substantially contributed to the 60-year increasing trend (Fig. 3, Table 4). The turning point, calculated by the sequential MK test, occurred approximately in 1993 (Fig. 4). Temporal changes of rainfall erosivity in the water erosion region (WE) were similar to the changes in China, probably because rainfall erosivity in NS and QT were the lowest nationwide and negligible, accounting for only a small fraction of the whole country.

It is noted that the 60-year temporal trends differed substantially for soil erosion regions. Two major groups can be classified: decreasing trends were found in NE, NS, N, NW and SW, whereas increasing trends were found in S, SK and QT (Table 4).

For regions with decreasing trends, three significance levels were determined: the 0.01 level, the 0.05 level and the insignificant level. The decreasing trend of region NW was significant at the 0.01 level (Table 4). Despite the increasing trends revealed for 1951–1960 and 1971–1980 and the significant trend in 1971–1980 at the 0.05 level, decreasing trends were reported for 4 decades in NW (Fig. 3, Table 4).

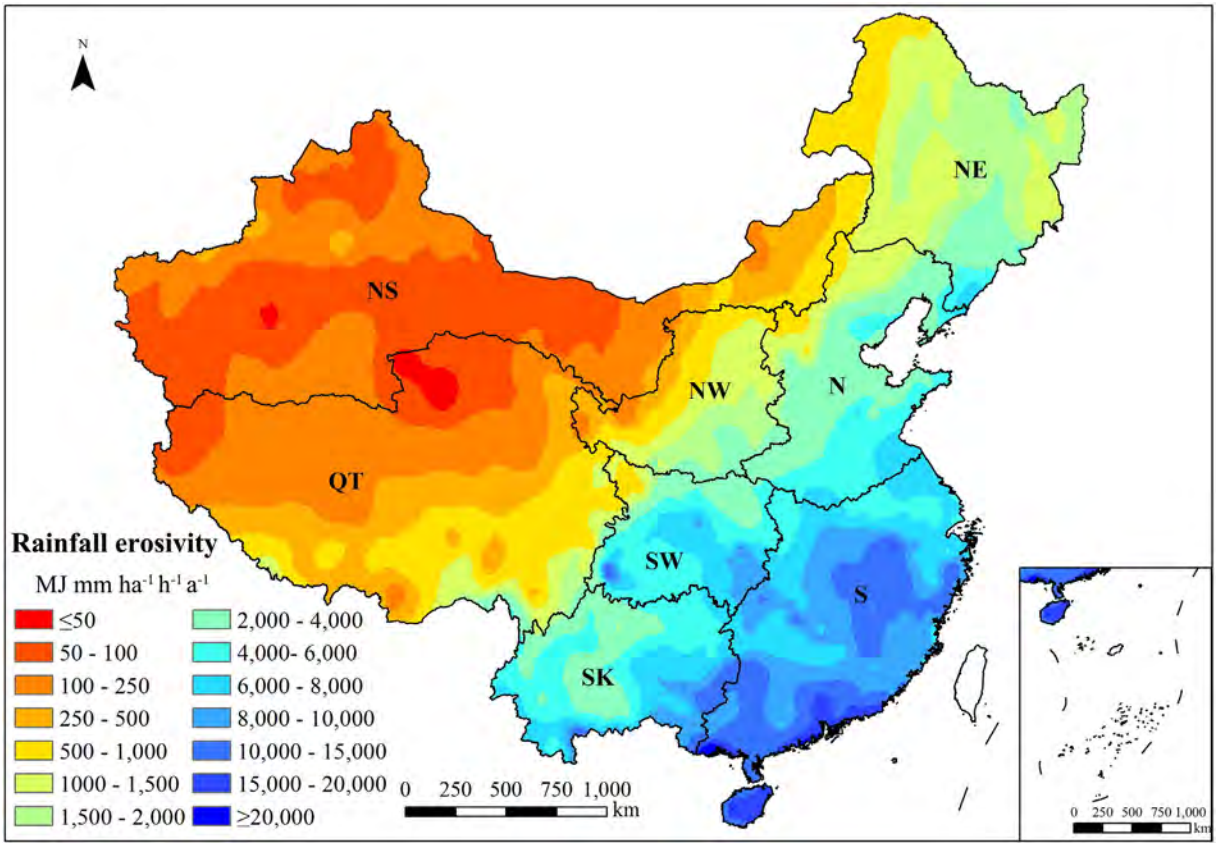

Fig. 2. Spatial distribution of 60-year average annual rainfall erosivity in mainland China.

Table 3
Rainfall erosivity of 60-year and different decades in mainland China and its soil erosion regions (MJ mm ha^{-1} h^{-1} a^{-1}).

	1951–1960	1961–1970	1971–1980	1981–1990	1991–2000	2001–2010	1951–2010
NE	1751.6	1636.2	1438.7	1742.9	1662.6	1433.5	1611.6
NS	172.3	147.8	157.4	149.3	174.2	150.2	158.5
N	3358.7	3389.3	9191.0	3070.2	3214.4	3170.9	3231.3
NW	1272.8	1238.6	1168.0	1135.4	1083.1	1110.7	1167.3
S	9340.3	9012.0	9355.9	9404.5	10,186.6	9581.8	9480.9
SW	5009.1	5113.7	5067.0	5389.4	4765.3	5010.9	5060.9
SK	5328.6	5638.3	5531.0	5336.6	5878.4	5600.4	5555.2
TP	412.6	400.3	393.2	416.5	404.2	420.7	407.6
WE	4509.0	4455.1	4424.2	4495.7	4682.4	4468.5	4506.4
CN	2440.0	2403.3	2388.5	2428.1	2527.1	2415.4	2433.9

Note: NE: northeast black soil region; NS: northern sandy region; N: northern rocky and earth mountain region; NW: northwest Loess Plateau region; S: southern red soil hilly region; SW: southwest purple soil region; SK: southwest Karst region; QT: Qinghai-Tibet Plateau region. WE: water erosion region; CN: mainland China.

Probably the longer decreasing period contributed greatly to the 0.01 level significant decreasing trend for 60-year rainfall erosivity in NW (Table 4). The turning point approximately occurred in 1982 (Fig. 4).

Significant decreasing trends at the 0.05 level were detected for NE and N (Table 4). However, the temporal change patterns for the two regions were quite different. The temporal trends of NE exhibited alternation from increasing to decreasing, followed by another period of increasing to decreasing to increasing. The significant decreasing trends of 1961 to 1970 (0.01 level) and 1971 to 1980 (0.1 level) substantially contributed to the total decreasing trend, despite the 0.05 level significant increasing trend of 1951 to 1960 (Table 4, Fig. 3). Three turning points were detected for the three alternating changes, which were approximately 1966, 1982 and 1998 (Fig. 4). Region N mainly displayed a decreasing trend (Table 4), except in the first and last decades of the 60-year period (Table 4, Fig. 3). The decreasing trends of four consecutive decades (1961–2000) contributed to the overall 60-year decreasing trend. The turning point approximately occurred in 1967 (Fig. 4).

The NS and SW regions showed no significant changes. Rainfall erosivity in NS was the lowest among all regions (Table 3, Fig. 2) due to the low rainfall in this region. Despite a significant increasing trend (0.01 level) for 2001–2010, temporal changes in NS were quite small for all other decades. An insignificant decreasing trend was detected for the 60-year period with a small Kendall slope, which was only −0.0055 (Table 4). No turning point was detected in this region (Fig. 4). Temporal changes of rainfall erosivity in SW were more complex than in NS. Rainfall erosivity decreased in three decades: 1951–1970 and 1981–1990, and also increased in three decades: 1971–1980 and 1991–2010 (Table 4, Fig. 3). Although the increasing trend was significant at the 0.05 level for 2001–2010, an insignificant trend was detected for the 60-year period, probably because the $|\beta|$ values for the decreasing decades were relatively higher than the increasing decades (Table 4). The turning point occurred approximately in 1987 (Fig. 4).

Increasing trends ($p < 0.05$) were found in S and SK. Although increasing trends and decreasing trends were both in three decades in S, similar to SW, a 0.05-level significant increasing trend was detected for S (Table 4), probably because the increasing trends were found in the last two decades and rainfall erosivity in the two decades was higher than in the previous decades (Table 3, Fig. 3). The turning point occurred in approximately 1989 (Fig. 4). SK displayed alternating trends for different decades, experiencing the following stages: decrease, increase (two decades), decrease, increase and decrease (Table 4, Fig. 3). Significant increasing trends were reported for two decades: the 0.05 level in 1961–1970 and 0.01 level in 1991–2000; and the significant decreasing trend was only found in 1981–1990 at the 0.05 level, finally 0.05-level significance was reported in this region (Table 4, Fig. 3). The turning points occurred approximately in 1965, 1985 and 1991 for SK (Fig. 4).

Despite increasing trends were observed for four decades (1971–2010), the overall increasing trend of QT was not significant (Table 4, Fig. 3), probably because two decades (1951–1970) showed decreasing trends, and the trend of one of these decades, 1951–1960, was significant at the 0.1 level (Table 4, Fig. 3). No turning point was detected for this region.

3.4. Spatial-temporal changes of rainfall erosivity

On the national scale, the Kendall slopes of 470 stations were positive, accounting for 62% of the total 756 stations; negative β values were reported for 286 stations, which is, 38% of the 756 stations. Substantial differences were found within the same regions, such as region NS, N, S, SW and SK (Fig. 5). Although decreasing trends were reported in region SW, many stations in the middle and eastern parts experienced increasing trends, with Kendall slopes higher than 10 for many stations. A similar phenomenon was reported in region N, despite the 0.05-level significant decreasing trend for the entire region, as an increasing trend was reported for the areas south of the Yellow River. Areas with decreasing trends were also observed within regions with

Table 4
Temporal trends of rainfall erosivity for mainland China and its soil erosion regions.

	1951–1960		1961–1970		1971–1980		1981–1990		1991–2000		2000–2010		1951–2010		
	z	β	z	β	z	β	z	β	z	β	z	β	z	β	Trend
NE	**2.40***	**20.3**	**−2.86****	**−50.4**	**−1.79**	**−21.6**	0.89	16.6	−1.07	−17.5	0.76	9.9	**−2.32**	**−3.89**	*↓
NS	0.94	2.8	1.07	2.9	0	−0.2	0	−0.03	1.07	1.7	1.77	1.7	0.05	−0.006	↓
N	0.31	9.4	−1.25	−76.0	**−2.15***	**−43.9**	0	−5.3	−0.54	−21.2	1.56	40.5	**−2.19**	**−4.56**	*↓
NW	1.15	42.9	−1.25	−9.8	**1.97***	**20.8**	−0.36	−5.4	−1.07	−12.3	−0.94	−22.6	**−4.13**	**−3.34**	**↓
S	−0.52	−38.1	0	6.8	−1.43	−106.1	−1.25	−93.3	1.43	109.8	0	5.1	**2.46**	**13.01**	*↑
SW	−0.94	−26.2	−1.07	−13.8	0.72	53.4	−1.25	−106.6	0.54	35.3	**1.98***	**75.1**	−0.97	−2.89	↓
SK	−1.15	−39.9	**2.50***	**110.4**	0.36	3.9	**−2.15***	**−64.1**	**3.58****	**89.3**	−0.10	−16.4	**2.16**	**5.91**	*↑
TP	**−1.77**	**−4.0**	−1.25	−0.6	0	1.6	**1.97***	**2.8**	**2.50***	**10.0**	1.36	4.8	1.19	0.21	↑
WE	0.10	3.1	−0.72	−12.5	−0.89	−15.4	−1.25	−14.6	**1.79**	**24.3**	0.31	6.4	0.82	0.81	↑
CN	0.10	3.1	−0.18	−12.5	−0.89	−15.4	−1.25	−14.6	**1.79**	**24.3**	0.31	6.4	0.68	0.50	↑

Note: Results in bold denote statistically significant at 0.1 significance level, in which, ** and * represent significance at 0.01 and 0.05 significance level, respectively. Positive β indicates the increasing trend and negative β indicates decreased trend.

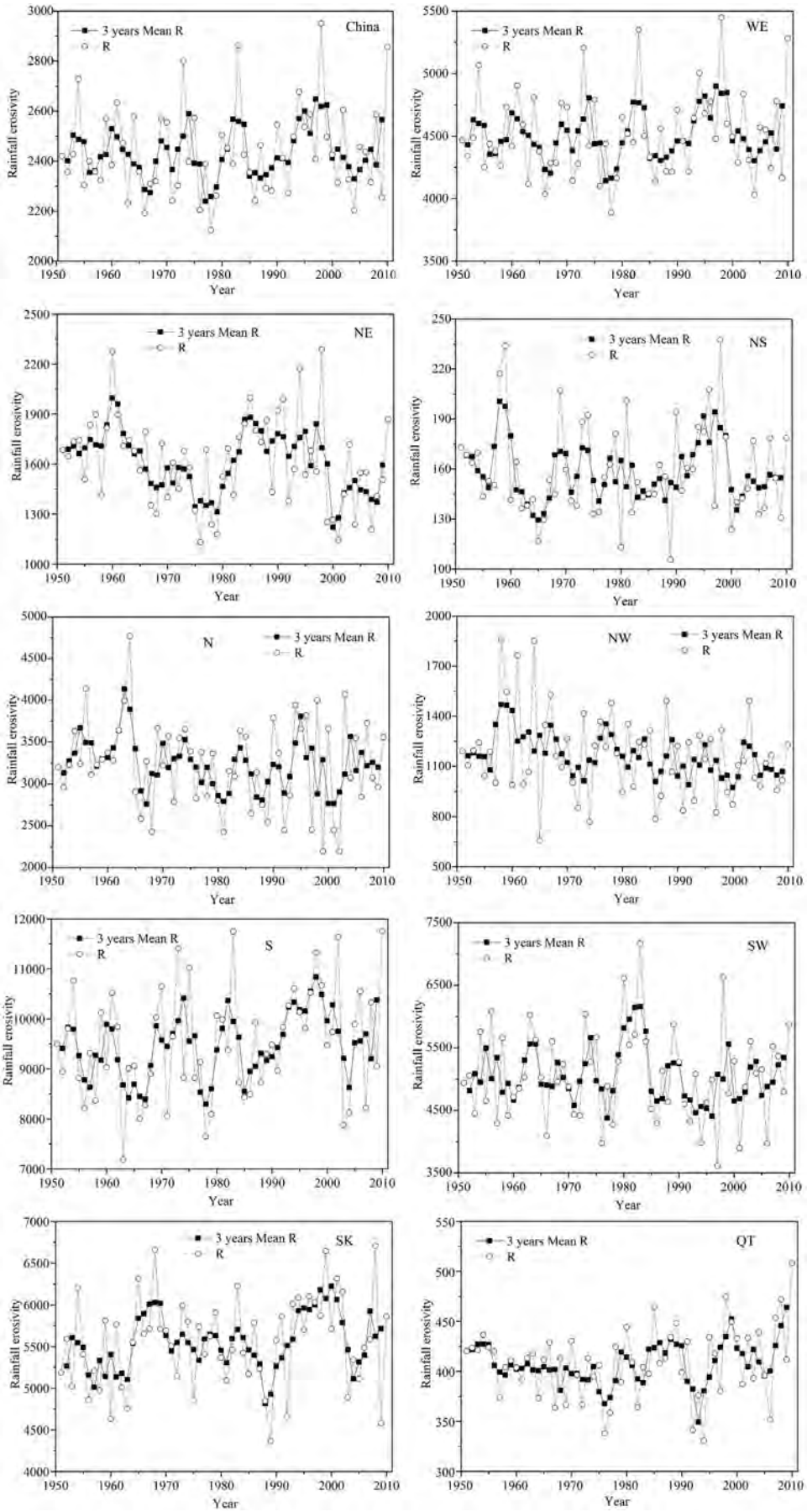

Fig. 3. Annual and 3-year moving average rainfall erosivity (MJ mm ha^{-1} h^{-1} a^{-1}) for mainland China and its soil erosion regions.

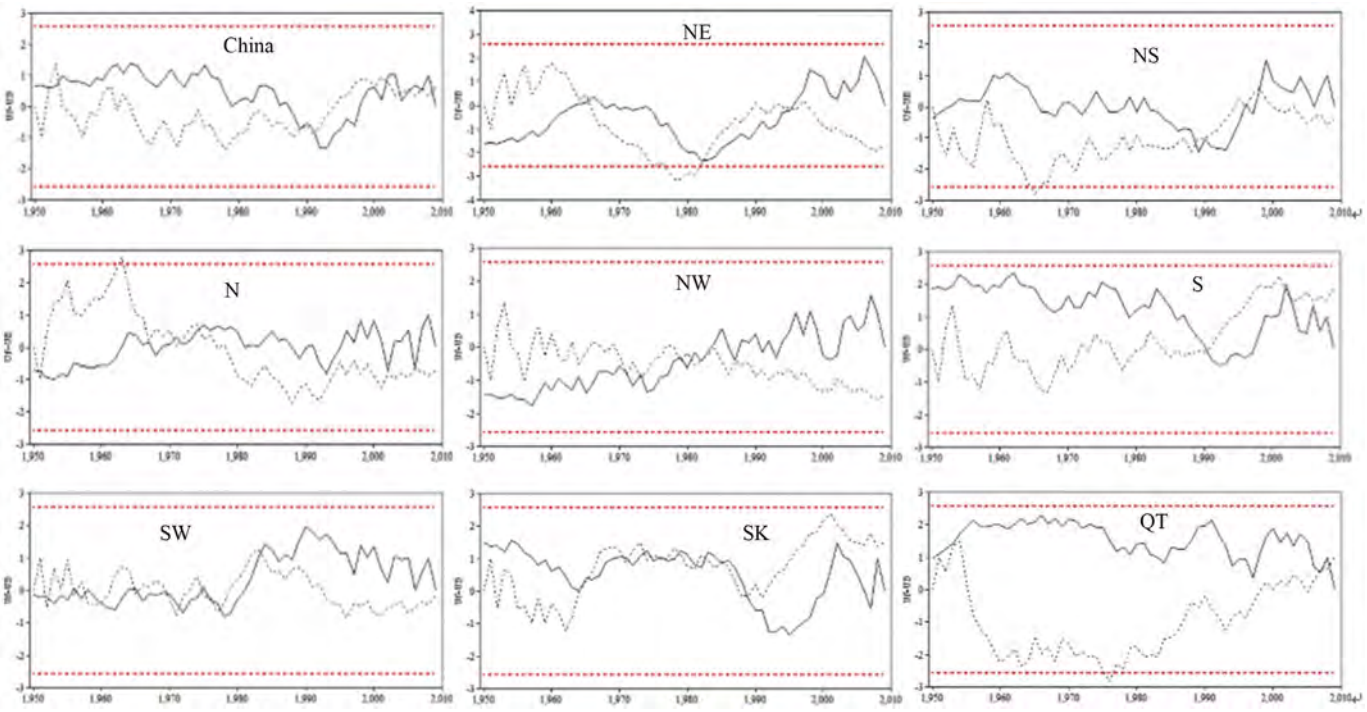

Fig. 4. Sequential MK test for 60-year rainfall erosivity of mainland China and its soil erosion regions.

increasing trends, such as the northern part of SK and the eastern part of S.

It can be concluded for most regions that the increasing or decreasing trends were determined by the trends of the majority of stations (Table 5). However, there are also exceptions in NS and SW. The percentage of stations with increasing trends in NS was 78%; however, an insignificant decreasing trend was reported for the entire region. This was probably because the β values for stations with $\beta > 0$ were quite small because these stations are mainly located in areas with very low rainfall erosivity, whereas stations with $\beta < 0$ are mainly in

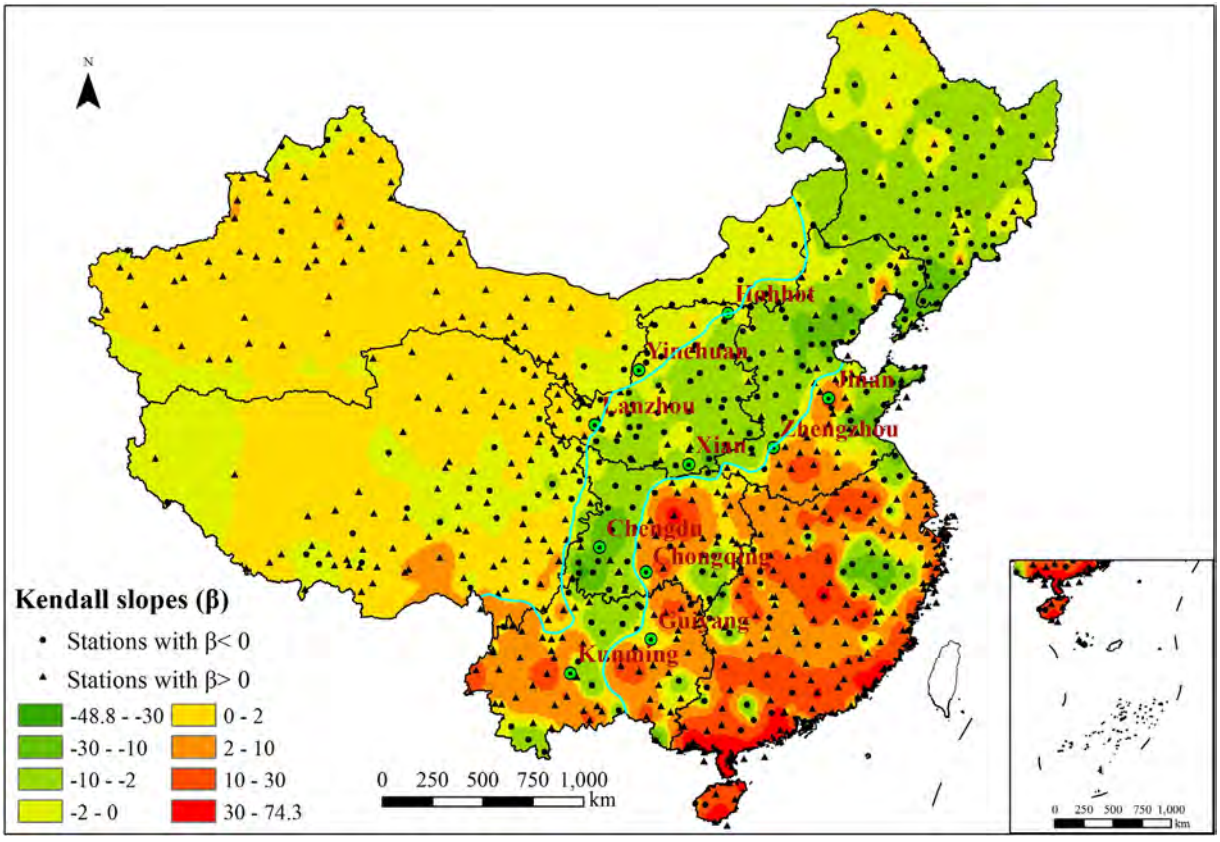

Fig. 5. Spatial distribution of Kendall slopes in mainland China.

Table 5
Percentage of stations with $\beta > 0$ and $\beta < 0$ in each soil erosion region.

Region	Number of stations	Percent of $\beta > 0$	Percent of $\beta < 0$	Region	Number of stations	Percent of $\beta > 0$	Percent of $\beta < 0$
NE	83	27.7	72.3	S	176	78.4	21.6
NS	89	77.5	22.5	SW	55	61.8	38.2
N	115	46.1	53.9	SK	72	72.2	27.8
NW	65	36.9	63.1	QT	101	76.2	23.8
WE	566	57.2	42.8	CN	756	62.2	37.8

the eastern area, with relatively higher rainfall erosivity and considerably higher $|\beta|$ values (Fig. 5). For SW, despite positive β values reported for 61.8% of stations (34 stations), this was offset by the much lower β values of the other 38.2% of stations (21 stations): for example, the βvalues for 11 stations were lower than −10, substantially reducing the regional β value.

Generally speaking, rainfall erosivity in the majority of China experienced an increasing trend with high spatial variability. The lowest β values were found in the western Sichuan Basin and the surrounding areas of the Bohai Sea, mainly Tianjin and Dalian, whereas the highest β values were found along the coastline of region S (Fig. 5). Obviously, a band of decreasing trends of rainfall erosivity extended in the northeast-southwest direction, including Northeast China, the Inner Mongolia Plateau, the North China Plain, the Loess Plateau, the western part of the Sichuan Basin and the northern part of the Yunnan-Guizhou Plateau. This band was surrounded by two lines consisting of capital cities of different provinces. The east line, that is, Jinan-Zhengzhou-Xian-Chongqing-Guiyang, delineated the eastern boundary of the decreasing area. The Hohhot-Yinchuan-Lanzhou-Chengdu-Kunming line served as the western boundary of the decreasing area (Fig. 5). The Kendall slopes of the vast area west of the band were much smaller than those of the eastern part (Fig. 5), and the temporal changes of rainfall erosivity were negligible during 1951–2010. This was consistent with the temporal pattern of precipitation from 1951 to 2010 in mainland China: the mean annual precipitation mainly decreased in northeast China, northern China and the Loess Plateau and mainly increased in south China (Gemmer et al., 2004; Zhang et al., 2009).

4. Discussion

In this study, the universal co-kriging method was selected as the best method from 16 interpolation methods to calculate the spatial distribution of rainfall erosivity from station-based weather data. Despite the comparison and selection of spatial interpolation methods were reported in some studies (Table 1), only several methods were considered in the comparison, which constrained these studies in terms of determining the most suitable interpolation method. In this study, 16 interpolation methods were compared, and the best method was selected for the country as a whole; thus, more studies exploring suitable methods for spatial interpolation for more regions are necessary.

Spatial-temporal changes of rainfall erosivity in China have been previously reported. Decreasing trends for northeast China, north China, the Loess Plateau and Sichuan Basin were reported by Liu et al. (2013a), whereas other regions experienced increasing trends, similar to the results in this study. However, spatial and temporal trends for soil erosion regions are lacking in this study. Spatial-temporal changes of rainfall erosivity at the regional scale in China have also been investigated. For example, rainfall erosivity of most weather stations located in the Yangtze River basin presented upward trends during 1960–2005 (Huang et al., 2013); significant decreasing trends from 1956 to 2008 were reported in the Loess Plateau (Xin et al., 2011; Abd Elbasit et al., 2013); and temporal changes of rainfall erosivity in the dryland region of China during 1961–2012 were reported by Yang and Lu (2015), indicating an upward trend for arid zone, a downward trend for sub-humid zone and no evident trend for the semi-arid zone. Results of the studies listed above were all similar with those of this study.

This study indicated that the temporal changes of rainfall erosivity for 1951–2010 in China were consistent with the changes of annual rainfall. Rainfall in northeast China, northern China, the Loess Plateau and Sichuan Basin showed decreasing trends (Gemmer et al., 2004; Zhang et al., 2009; Xin et al., 2011; Abd Elbasit et al., 2013), whereas increasing trends were reported in South China, northwest China and the Qinghai-Tibet Plateau (Gemmer et al., 2004; Zhang et al., 2009). The time period of the studies listed above was all from the 1950s to 2000s, similar to this study. The correspondence of rainfall and rainfall erosivity implies that the temporal changes of rainfall erosivity, to some degree, were determined by the temporal changes of rainfall.

Temporal changes of rainfall erosivity over the past 60 years can also reflect future scenarios, which has important implications for soil conservation and land use planning. They can also provide guidance for future research and soil conservation efforts. For example, a decrease in rainfall erosivity of NW is helpful for reducing soil erosion; however, the decrease in rainfall will also exert a potential negative effect on ecological restoration because water resource is an important limiting factor in NW (Xin et al., 2011). Thus, efforts to conserve rainfall or water resource should be emphasized. For regions with increasing trends, such as SK and S, soil conservation measures should be taken to reduce the potential higher degree soil erosion caused by increasing rainfall erosivity and these measures should be mainly deployed on slope farmlands and orchards because these land use types were more susceptible to soil erosion.

Quantifying the temporal change of rainfall erosivity is essential for accurately assessing the effects of soil conservation measures. For example, the sediment load of the Yellow River has decreased substantially from the 1950s to 2010s: the annual sediment load of the Yellow River of 1951 to 1979, 1980 to 1999 and 2000 to 2010 were 1.34, 0.73 and 0.32 Gt yr^{-1} (Wang et al., 2015), respectively; the annual sediment discharge of the Yellow River for each decade from 1950 to 2008 was 1.76, 1.48, 1.37, 0.83, 0.84 and 0.38 Gt yr^{-1} (Mu et al., 2012), respectively. Considering the Loess Plateau was the source of nearly 90% of the Yellow River's sediment load (Wang et al., 2015) and soil conservation measures were widely adopted in the Loess Plateau since the 1970s, it can be concluded that the reduction of sediment load was contributed to the combined effects of both the widely implemented soil conversation measures in the Loess Plateau and the decreasing trend of rainfall erosivity in NW (Fig. 5) Wang et al. (2015) concluded that decreased rainfall contributed to 22% of the reduction of sediment load from 1951 to 1979 to 1980–1999, 4% from 1980 to 1999 to 2000–2010. Mu et al. (2012) also concluded that the effect of rainfall on the sediment discharge decline was 14, 24 and 17% for the 1980s, 1990s and 2000s, respectively. Both results indicated that approximately 80% of the sediment load decline was contributed by soil conservation measures, implying that it is necessary to understand the temporal change of rainfall erosivity to accurately assess the effects of soil conservation measures.

Changes of the sediment load of the main rivers in China during 1955–2010 were reported by Liu et al. (2013b), and the decrease ratios for the Yangtze, Yellow, Pearl, Haihe, Huaihe and Liaohe Rivers were −1.5%, −3.2%, −1.1%, −12.2%, −3.6% and −2.7%, respectively. It can be observed that although rainfall erosivity for the majority region of the Yangtze, Pearl and Huaihe Basins increased from 1951 to 2010, the sediment load of these rivers decreased in the same period, implying that soil conservation measures in these regions exhibited positive effects in reducing soil erosion, and these effects have overcame the potential increase of soil loss induced by the increasing rainfall erosivity. The decreased sediment loads in the Yellow, Liaohe and Haihe Rivers were probably the result of the combined effects of decreased rainfall erosivity and soil conservation measures.

5. Conclusions

The spatial and temporal distributions of rainfall erosivity in mainland China and soil erosion regions from 1951 to 2010 were analyzed using daily rainfall data from 756 weather stations. It is concluded that the universal co-kriging method was the most suitable method for China. Based on the rainfall patterns, the rainfall erosivity increased from the northwest to the southeast, from 30.7 to 30,051.1 MJ mm ha^{-1} h^{-1} a^{-1}. The overall rainfall erosivity did not change across China and its soil erosion regions. However, both decreasing and increasing trends were observed in northern and southern China, respectively. Within a given soil erosion region, substantial spatial differences in temporal changes of rainfall erosivity were observed. This study indicated that knowing the temporal trends of rainfall erosivity is essential for accurately assessing the effects of soil conservation measures on soil erosion.

Future studies should relate the trends of rainfall erosivity detected from this study to sediment loading in major rivers across China to further evaluate the usefulness of rainfall erosivity in evaluating potential soil erosion at the large basin to regional scale. Additionally, this study provides a method and baseline to study the impacts of anticipated climate change on spatial and temporal change in rainfall erosivity and soil erosion in China.

Acknowledgements

This study was funded by the Commonwealth Research Program of the Ministry of Water Resources (No. 200901047), National Basic Research Program of China (973 Program) (No. 2015CB452704) and the National Natural Science Foundation of China (No. 31200535).

References

Abd Elbasit, M.A.M., Huang, J.B., Ojha, C.S.P., Yasuda, H., Adam, E.O., 2013. Spatiotemporal changes of rainfall erosivity in loess plateau. China, ISRN Soil Sci. 2013, 1–8.
Angulo-Martínez, M., Beguería, S., 2012. Trends in rainfall erosivity in NE Spain at annual, seasonal and daily scales, 1955–2006. Hydrol. Earth Syst. Sci. 16 (10), 3551–3559.
Angulo-Martínez, M., López-Vicente, M., Vicente Serrano, S.M., Beguería, S., 2009. Mapping rainfall erosivity at a regional scale: a comparison of interpolation methods in the Ebro Basin (NE Spain). Hydrol. Earth Syst. Sci. 13, 1907–1920.
Bonilla, C.A., Vidal, K.L., 2011. Rainfall erosivity in Central Chile. J. Hydrol. 410, 126–133.
Gemmer, M., Becker, S., Jiang, T., 2004. Observed monthly precipitation trends in China 1951–2002. Theor. Appl. Climatol. 77, 39–45.
Goovaerts, P., 1999. Using elevation to aid the geostatistical mapping of rainfall erosivity. Catena 34, 227–242.
Hoyos, N., Waylen, P.R., Jaramillo, Á., 2005. Seasonal and spatial patterns of erosivity in a tropical watershed of the Colombian Andes. J. Hydrol. 314, 177–191.
Huang, J., Zhang, J.C., Zhang, Z.X., Xu, C.Y., 2013. Spatial and temporal variations in rainfall erosivity during 1960–2005 in the Yangtze River basin. Stoch. Env. Res. Risk A. 27, 337–351.
Hudson, N.W., 1995. Soil Conservation (3rd Edition). Iowa State University Press, Ames, Iowa, p. 25.
Liu, B.T., Tao, H.P., Song, C.F., Guo, B., Shi, Z., Zhang, C., Kong, B., He, B., 2013a. Temporal and spatial variations of rainfall erosivity in China during 1960 to 2009. Geogr. Res. 32 (2), 245–256 (In Chinese with English Abstract).
Liu, C., Sui, J.Y., He, Y., Hirshfield, F., 2013b. Changes in runoff and sediment load from major Chinese rivers to the Pacific Ocean over the period 1955–2010. Int. J. Sediment Res. 28 (4), 486–495.
Lu, H., Yu, B.F., 2002. Spatial and seasonal distribution of rainfall erosivity in Australia. Aust. J. Soil Res. 40, 887–901.
Ma, X., He, Y.D., Xu, J.C., van Noordwijk, M., Lu, X.X., 2014. Spatial and temporal variation in rainfall erosivity in a Himalayan watershed. Catena 121, 248–259.
Mann, H.B., 1945. Nonparametric tests against trend. Econometrica 245–259.
Men, M.X., Yu, Z.R., Xu, H., 2008. Study on the spatial pattern of rainfall erosivity based on geostatistics in Hebei Province, China. Front. Agric. China 2 (3), 281–289.
Meusburger, K., Steel, A., Panagos, P., Montanarella, L., Alewell, C., 2012. Spatial and temporal variability of rainfall erosivity factor for Switzerland. Hydrol. Earth Syst. Sci. 16, 167–177.
Mitchell, J.M., Dzerdzeevskii, B., Flohn, H., Hofmeyr, W.L., Lamb, H.H., Rao, K.N., Wallen, C.C., 1966. Climate Change, WMO Technical Note No.79. World Meteorological Orgazination, p. 79.
Morgan, P.R.C., 2005. Chapter 4. Erosion Hazard Assessment. Soil Erosion and Conservation, third ed. Blackwell Publishing, London, p. 67.
Mu, X.M., Zhang, X.Q., Shao, H.B., Gao, P., Wang, F., Jiao, J.Y., Zhu, J.L., 2012. Dynamic changes of sediment discharge and the influencing factors in the Yellow River, China, for the recent 90 years. Clean-Soil, Air Water 40 (3), 303–309.
Nash, J.E., Sutcliffe, J.V., 1970. River flow forecasting through conceptual models. Part I — a discussion of principles. J. Hydrol. 10 (3), 282–290.
Nearing, M.A., 2001. Potential changes in rainfall erosivity in the US with climate change during the 21st century. J. Soil Water Conserv. 56 (3), 229–232.
Nearing, M.A., Pruski, F.F., O'Neal, M.R., 2004. Expected climate change impacts on soil erosion rates: a review. J. Soil Water Conserv. 59 (1), 43–50.
Renard, K.G., Foster, G.R., Weesies, G.A., McCool, D.K., Yoder, D.C., 1997. Predicting soil erosion by water: a guide to conservation planning with the revised universal soil loss equation (RUSLE). Agriculture Handbook 703. US Department of Agriculture, Washington, DC.
Sauerborn, P., Klein, A., Botschek, J., Skowronek, A., 1999. Future rainfall erosivity derived from large-scale climate models: methods and scenarios for a humid region. Geoderma 93 (3–4), 269–276.
Segura, C., Sun, G., McNulty, S.G., Zhang, Y., 2014. Potential impacts of climate change on soil erosion vulnerability across the conterminous United States. J. Soil Water Conserv. 69 (2), 171–181.
de Silva, A.M., 2004. Rainfall erosivity map for Brazil. Catena 57, 251–259.
Sun, G., McNulty, S.G., Moore, J., Bunch, C., Ni, J., 2002. Potential impacts on climate change on rainfall erosivity and water availability in China in the next 100 years. Proceedings of the 12th International Soil Conservation Conference, Beijing, China, 2002.
Sneyers, R., 1990. On the statistical analysis of series of observations, 143. World Meteorol. Organ. Genava 192.
Wang, C.H., Li, J., Li, X.L., Xu, X.G., 2012. Analysis on quasi-periodic characteristics of precipitation in recent 50 years and trend in next 20 years in China. Arid Zone Res. 29 (1), 1–10 (In Chinese with English Abstract).
Wang, S., Fu, B.J., Piao, S.L., Lv, Y.H., Ciais, P., Feng, X.M., Wang, Y.F., 2015. Reduced sediment transport in the Yellow River due to anthropogenic changes. Nat. Geosci. (http://www.nature.com/ngeo/journal/vaop/ncurrent/full/ngeo2602.html).
Williams, J., Nearing, M.A., Nicks, A., Skidmore, E., Valentine, C., King, K., Savbi, R., 1996. Using soil erosion models for global change studies. J. Soil Water Conserv. 51 (5), 381–385.
Wischmeier, W.H., Smith, D.D., 1965. Predicting rainfall erosion losses from cropland east of the Rocky Mountains. Agriculture Handbook. No. 282. US Department of Agriculture, Washington, DC.
Wischmeier, W.H., Smith, D.D., 1978. Predicting rainfall erosion losses: a guide to conservation planning. Agriculture Handbook. No. 537. US Department of Agriculture, Washington, DC.
Xiao, M.Z., Zhang, Q., Singh, V.P., Chen, X.H., 2013. Regionalization-based spatiotemporal variations of precipitation regimes across China. Theor. Appl. Climatol. 114, 203–212.
Xin, Z.B., Yu, X.X., Li, Q.Y., Lu, X.X., 2011. Spatial-temporal variation in rainfall erosivity on the Chinese loess plateau during the period 1956–2008. Reg. Environ. Chang. 11, 149–159.
Xu, Z.X., Takeuchi, K., Ishidaira, H., 2003. Monotonic trend and step changes in Japanese precipitation. J. Hydrol. 279 (1), 144–150.
Yang, F.B., Lu, C.H., 2015. Spatiotemporal variation and trends in rainfall erosivity in China's dryland region during 1961-2012. Catena 133, 362–372.
Yue, S., Pilon, P., Cavadias, G., 2002. Power of the Mann-Kendall and Spearman's rho tests for detecting monotonic trends in hydrologic series. J. Hydrol. 259, 254–271.
Zhang, G.H., Nearing, M.A., Liu, B.Y., 2005. Potential effects of climate change on rainfall erosivity in the Yellow River basin of China. Trans. ASAE 48 (2), 511–517.
Zhang, Q., Xu, C.Y., Zhang, Z., Chen, Y.D., Liu, C.Y., 2009. Spatial and temporal variability of precipitation over China, 1951-2005. Theor. Appl. Climatol. 95, 53–68.
Zhang, W.B., Fu, J.S., 2003. Rainfall erosivity estimation under different rainfall amount. Resour. Sci. 25 (1), 35–41 (In Chinese with English Abstract).
Zhang, W.B., Xie, Y., Liu, B.Y., 2002. Rainfall erosivity estimation using daily rainfall amounts. Sci. Geogr. Sin. 22, 705–711 (In Chinese).
Zheng, J., Li, G.Y., Han, Z.Z., Meng, G.X., 2010. Hydrological cycle simulation of an irrigation district based on a SWAT model. Math. Comput. Model. 51, 1312–1318.
Zhu, Z., Yu, B., 2015. Validation of rainfall erosivity estimators for mainland China. Trans. ASABE 58 (1), 61–71.